

Physics-Infused Reduced-Order Modeling for Analysis of Ablating Hypersonic Thermal Protection Systems

October 10, 2025

Abstract

This work presents a physics-infused reduced-order modeling (PIROM) framework towards the design, analysis, and optimization of non-decomposing ablating hypersonic thermal protection systems (TPS).

1 Introduction

At hypersonic speeds, aerospace vehicles experience extreme aero-thermal environments that requires specialized thermal protection systems (TPS) to shield internal sub-structures, electronics, and possibly crew members from the intense aerodynamic heating. The TPS is often composed of ablating materials – a high-temperature capable fibrous material injected with a resin that fills the pore network and strengthens the composite [Amar2016](#). The TPS design promotes the exchange of mass through thermal and chemical reactions (i.e., pyrolysis), effectively mitigating heat transfer to the sub-structures.

As a result, accurate prediction for the ablating TPS response under extreme hypersonic heating becomes fundamental to ensuring survivability, performance, and safety of hypersonic vehicles. Not only is it necessary to assess the performance of the thermal management systems, but also the shape changes of the vehicle’s outer surface induced by the ablating material, and its impact on the aerodynamics, structural integrity, and controllability. Unfortunately, high-fidelity simulations of ablating TPS remains a formidable challenge both theoretically and computationally.

On the theoretical side, the thermo-chemical reactions, coupled with the irregular pore network structure, translate into simplifying assumptions to reduce non-linearities, and make the resulting equations more amenable for engineering application and design analysis [x](#). For instance, one of the most notable codes is the one-dimensional [CMA](#) code that was

developed by Aerotherm Corporation in the 1960s [Howard2015](#). Despite its practical use in...

Another example is the CHarring Ablator Response (CHAR) ablation code, which ignores elemental decompositions of the pyrolyzing gases, assumes the gases to be a mixture of perfect gases in thermal equilibrium, and assumes no reaction or condensation with the porous network [?].

theoretically:

computationally:

2 Modeling of Ablating Thermal Protection Systems

This section presents the problem of modeling ablation for a non-decomposing TPS as a parametrized system of coupled non-linear PDEs. The ablation physics is decomposed into heat conduction and mesh motion, which are governed by the energy and pseudo-elasticity PDEs, respectively. Predictions for the ablating TPS response computed based on two models: (1) a high-fidelity FOM based on discontinuous Galerkin FEM (DG-FEM), and (2) an RPM based on the LCM. The mathematical details for the governing equations, FOM, and RPM, are provided next.

2.1 Governing Equations

Heat Conduction Consider a generic domain $\Omega \subset \mathbb{R}^d$, $d = 2$ or 3 , illustrated in Fig. 1. Let $\partial\Omega = \Gamma_q \cup \Gamma_T$ and $\Gamma_q \cap \Gamma_T = \emptyset$, where a Neumann $q_b(x, t)$ boundary condition is prescribed on the Γ_q boundary, and a Dirichlet $T_b(x, t)$ boundary condition is prescribed on the boundary Γ_T . The ablation is modeled as mesh motion, and occurs only on the heated boundary Γ_q . Ablating effects on the energy equation are handled using the Arbitrary Lagrangian-Eulerian (ALE) description. The ALE establishes that mesh displacements $w(x, t) \in \mathbb{R}^d$ and velocities $v(x, t) \in \mathbb{R}^d$ evolve independently of the physical material's displacements, which are set to zero [CITE](#).

The transient heat conduction is described by the energy equation,

$$\rho c_p \left(\frac{\partial T}{\partial t} - v(x, t) \cdot \nabla T \right) - \nabla \cdot (\mathbf{k} \nabla T) = \mathcal{Q}(x, t), \quad x \in \Omega \quad (1a)$$

$$-\mathbf{k} \nabla T \cdot \mathbf{n} = q_b(x, t), \quad x \in \Gamma_q \quad (1b)$$

$$T(x, t) = T_b(x, t), \quad x \in \Gamma_T \quad (1c)$$

$$T(x, 0) = T_0(x), \quad x \in \Omega \quad (1d)$$

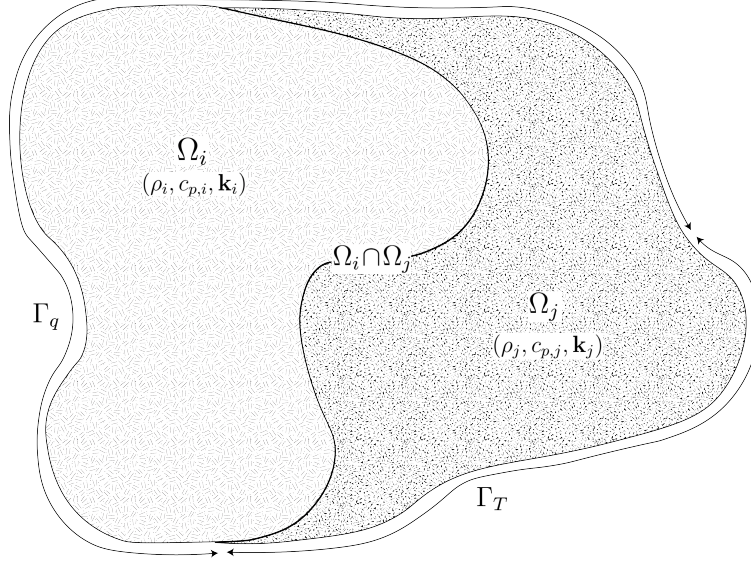


Figure 1: General domain Ω with prescribed Neumann and Dirichlet boundary conditions on Γ_q and Γ_T . Mesh displacement $w(x, t)$ occurs on the Γ_q boundary.

54 where the density ρ is constant, while the heat capacity c_p and thermal conductivity $\mathbf{k} \in$
55 $\mathbb{R}^{d \times d}$, are temperature dependent. In the order they appear, the terms in eq. (1a) include,
56 the unsteady energy storage, heat conduction, temperature advection due to mesh motion,
57 and source terms due to boundary conditions.

58 **Mesh Motion** The mesh motion is described by the pseudo-elasticity equation,

$$\nabla \cdot \sigma(w) = 0 \quad (2a)$$

$$w(x, t) = w_q(x, t), \quad x \in \Gamma_q \quad (2b)$$

$$w(x, t) = 0, \quad x \notin \Gamma_q \quad (2c)$$

$$w(x, 0) = \mathbf{0} \quad (2d)$$

59 where the stress tensor σ is related to the strain tensor $\epsilon(w)$ through Hooke's law,

$$\sigma(w) = \mathbb{D} : \epsilon(w)$$

60 where \mathbb{D} is the constitutive operator, “:” is the double contraction of tensors, and ϵ is the
61 symmetric strain tensor given by,

$$\epsilon(\mathbf{w}) = \frac{1}{2} (\nabla \mathbf{w} + \nabla \mathbf{w}^T)$$

For instance, an isotropic material assumption results in,

$$\boldsymbol{\sigma} = \lambda (\nabla \cdot \mathbf{w}) \mathbf{I} + 2\mu \boldsymbol{\epsilon}(\mathbf{w})$$

where λ and μ are Lamé constants that are arbitrarily selected to model the mesh motion. The “material” properties λ and μ can be chosen to tailor the mesh deformation and need not represent the actual material being modeled [Amar2016](#).

The boundary conditions for the energy equation includes a heated surface (eq. (1b)) and a constant-temperature surface (eq. (1c)). The boundary conditions for the pseudo-elasticity equation are a function of the surface temperature $T_q(x, t)$ for $x \in \Gamma_q$ on the heated boundary. For the i -th component, the surface velocities are imposed based on the following relation,

$$\hat{\mathbf{n}} \cdot \mathbf{v}(x, t) = f(T_q(x, t)) \quad (3)$$

where $\hat{\mathbf{n}}$ is the unit normal vector on the heated boundary Γ_q , and f is a function obtained from tabulated data for the material, commonly referred to as a B’ table. The B’ table provides the recession velocity as a function of surface temperature, and is pre-computed based on high-fidelity simulations of the ablation process for a one-dimensional slab of the material, and is independent of the TPS geometry and boundary conditions. The surface displacements are then computed by integrating the surface velocities over time,

$$\mathbf{w}_q(x, t) = \int_0^t \mathbf{v}(x, \tau) d\tau = \int_0^t \mathbf{f}(T_q(x, \tau)) d\tau \quad (4)$$

2.2 Full-Order Model: Finite-Element Method

To obtain the full-order numerical solution, the governing equation is spatially discretized using variational principles of Discontinuous Galerkin (DG) to result in a high-dimensional system of ordinary differential equations (ODEs). Note that the choice of DG approach here is mainly for theoretical convenience in the coarse-graining formulation, and is exclusively performed on the energy equation as the quantities of interest correspond to the ablating surface temperatures. In Sec. [x](#), the high-fidelity ablating TPS solution is performed using standard FEM for both the energy and elasticity equations, and the equivalence between DG and standard FEM is noted upon their convergence.

Consider a conforming mesh partition domain, where each element belongs to one and only one component. Denote the collection of all M elements as $\{E_i\}_{i=1}^M$. In an element E_i , its shared boundaries with another element E_j , Neumann BC, and Dirichlet BC are denoted as e_{ij} , e_{iq} , and e_{iT} , respectively. Lastly, $|e|$ denotes the length ($n_d = 2$) or area ($n_d = 3$) of a

89 component boundary e .

90 For the i -th element, use a set of P trial functions, such as polynomials, to represent the
91 temperature distribution,

$$T^{(i)}(x, t) = \sum_{l=1}^P \phi_l^{(i)}(x) u_l^{(i)} \equiv \boldsymbol{\phi}^{(i)}(x)^T \mathbf{u}^{(i)}(t), \quad i = 1, 2, \dots, M \quad (5)$$

92 By standard variational processes, e.g., [Cohen2018](#), the element-wise governing equation is
93 denoted as,

$$\mathbf{A}^{(i)} \dot{\mathbf{u}}^{(i)} = (\mathbf{B}^{(i)} + \mathbf{C}^{(i)}) \mathbf{u}^{(i)} + \sum_{j \in \mathcal{N}_i \cup \{T_b\}} \left(\mathbf{B}_{ij}^{(i)} \mathbf{u}^{(i)} + \mathbf{B}_{ij}^{(j)} \mathbf{u}^{(j)} \right) + \mathbf{f}^{(i)}(t), \quad \text{for } i = 1, 2, \dots, M \quad (6)$$

94 which is collected as the following ODE for the all the elements in the mesh,

$$\mathbf{A}(\mathbf{u}) \dot{\mathbf{u}} = [\mathbf{B}(\mathbf{u}) + \mathbf{C}(\mathbf{u})] \mathbf{u} + \mathbf{f}(t) \quad (7)$$

95 where $\mathbf{u} = [\mathbf{u}^{(1)}, \mathbf{u}^{(2)}, \dots, \mathbf{u}^{(M)}]^T \in \mathbb{R}^{MP}$ includes all the DG variables, $\mathbf{f} \in \mathbb{R}^{MP}$ is the
96 external forcing, and the system matrices \mathbf{A} , \mathbf{B} , and \mathbf{C} are the matrices due to heat capacity,
97 heat conduction, and temperature advection due to mesh motion, respectively. A detailed
98 derivation of eqs. (6) and (7) and their matrices is provided in Appendix [?].

99 2.3 Reduced-Physics Model

100 The RPM for predicting the response of the ablating TPS consists of two components: (1) the
101 LCM, and (2) tabulated data for ablating velocity as a function of surface temperature. The
102 LCM is described as a first-order system of ODEs for predicting the average temperatures
103 inside the ablating TPS, and provides a low-fidelity under-estimation for the ablating surface
104 temperature. The temperature prediction from LCM is used in a B' table to determine the
105 surface recession velocity, from which the displacements are obtained through integration.

106 2.3.1 Lumped Capacitance Model

107 The main results regarding the LCM are provided in this section; details of the implementa-
108 tion for the TPS in Fig. 2 are provided in Appendix A. The LCM is a classical physics-based
109 low-order model for predicting the temporal variation of average temperature in multiple in-
110 terconnected components [INCROPERA](#). The LCM is derived at the component level from
111 a point of view of energy conservation, and leads to the following system of ODEs for the

112 average temperatures on the components,

$$\bar{\mathbf{A}} \dot{\bar{\mathbf{u}}} = \bar{\mathbf{B}} (\bar{\mathbf{u}}) \bar{\mathbf{u}} + \bar{\mathbf{f}}(t) \quad (8)$$

113 where,

$$\bar{\mathbf{u}} = [\bar{u}^{(1)}, \bar{u}^{(2)}, \dots, \bar{u}^{(N)}]^T \in \mathbb{R}^N \quad (9a)$$

$$\bar{\mathbf{f}} = [\bar{f}^{(1)}, \bar{f}^{(2)}, \dots, \bar{f}^{(N)}]^T \in \mathbb{R}^N \quad (9b)$$

114 includes the average temperatures $\bar{\mathbf{u}}$ and forcing inputs $\bar{\mathbf{f}}$ for the N components. For $i, j =$
 115 $1, 2, \dots, N$ the (i, j) -th elements of the $\bar{\mathbf{A}} \in \mathbb{R}^{N \times N}$, $\bar{\mathbf{B}} \in \mathbb{R}^{N \times N}$, and $\bar{\mathbf{f}} \in \mathbb{R}^N$ matrices are
 116 given by,

$$\bar{A}^{(i)} = \begin{cases} \int_{\Omega^{(i)}} \rho c_p d\Omega^{(i)}, & i = j \\ 0, & i \neq j \end{cases}, \quad \bar{B}_{ij} = \begin{cases} \sum_{j \in \mathcal{N}_i \cup \{T_b\}} \bar{B}_{ij}^{(i)}, & i = j \\ \bar{B}_{ij}^{(j)}, & i \neq j \end{cases}, \quad (10a)$$

$$\mathbf{f}^{(i)} = \begin{cases} |e_{iq}| \bar{q}^{(i)} + \frac{|e_{iT}|}{R_i} \bar{T}^{(i)}, & i = j \\ 0, & i \neq j \end{cases} \quad (10b)$$

117 where,

$$\bar{q}^{(i)} = \frac{1}{|e_{iq}|} \int_{e_{iq}} q_b de_{iq}, \quad \bar{T}^{(i)} = \frac{1}{|e_{iT}|} \int_{e_{iT}} T_b de_{iT}, \quad \bar{B}_{ij}^{(i)} = -\frac{|e_{ij}|}{R_{ij}}, \quad \bar{B}_{ij}^{(j)} = \frac{|e_{ij}|}{R_{ij}} \quad (11)$$

118 2.3.2 Surface Recession Velocity and Displacements

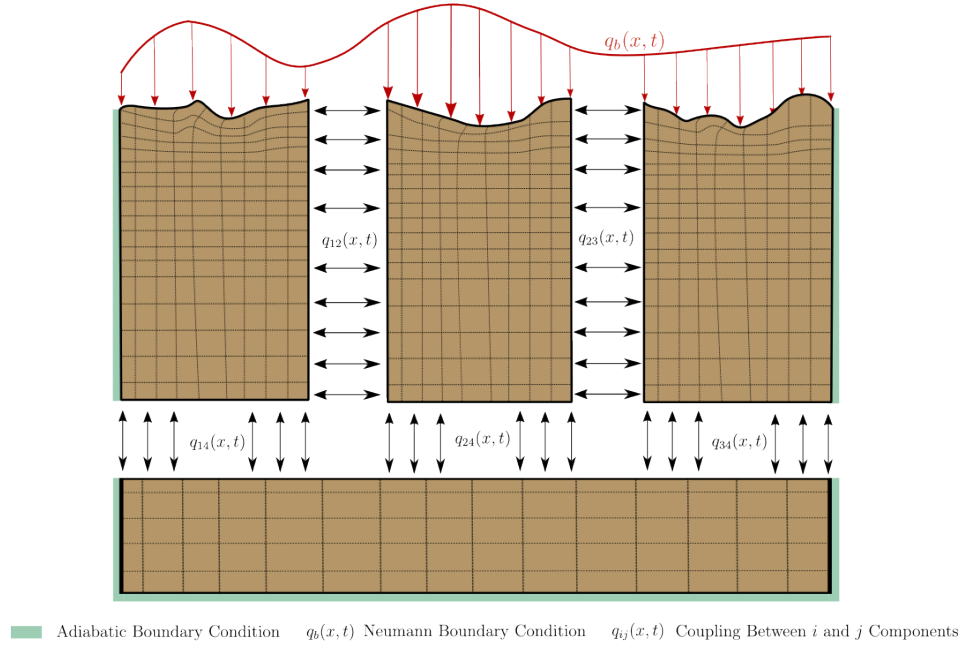
119 The surface velocity on the heated boundary Γ_q is computed based on the temperature
 120 predicted by the LCM using eq. (3). Thus, based on the i -th average temperature $\bar{u}^{(i)}$, the
 121 wall-normal surface velocity is computed as,

$$\hat{\mathbf{n}} \cdot \mathbf{v}^{(i)}(x, t) = f(\bar{u}^{(i)}(t)) \quad (12)$$

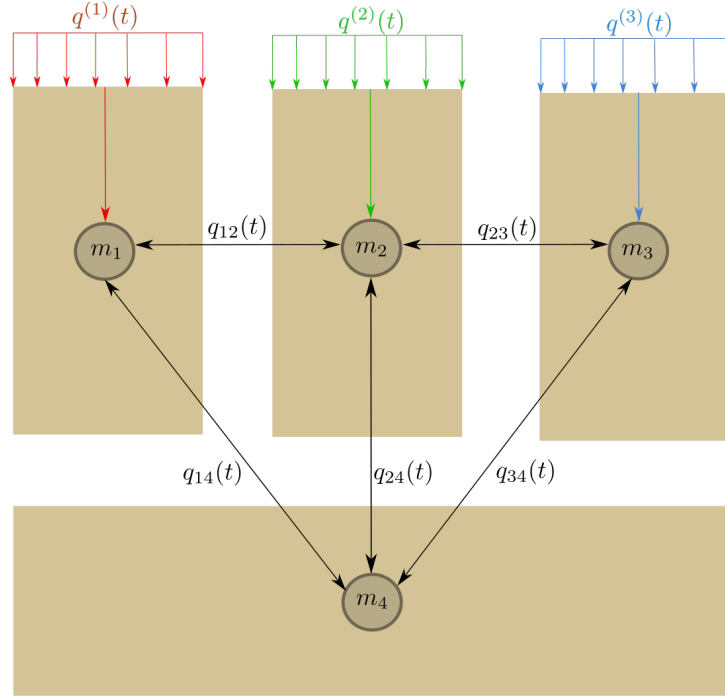
122 Due

123 2.4 Summary of Modeling Approaches

124 The FOM (i.e., DG-FEM) and RPM (i.e., LCM) are two different but mathematically con-
 125 nected solution strategies. Specifically, the LCM in eq. (8) not only resembles the functional



(a) TPS Decomposition



(b) Lumped Mass Representation

Figure 2: Partition of the TPS into three ablating and one non-ablating components with the corresponding lumped-mass representation.

form of the DG model in eq. (7), but can be viewed as a special case of the latter, where the mesh partition is extremely coarse, and the trial and test functions are piece-wise constants. For example, consider the case where each component $\Omega^{(i)}$ is treated as one single element, and each element employs one constant basis function $\phi^{(i)} = 1$. The element-wise DG model in eq. (6) simplifies into a scalar ODE that ignores advection effects due to mesh motion,

$$\mathbf{A}^{(i)} = \bar{A}^{(i)}, \quad \mathbf{C}^{(i)} = 0, \quad \mathbf{B}_{ij}^{(i)} = -\sigma|e_{ij}|, \quad \mathbf{B}_{ij}^{(j)} = \sigma|e_{ij}|, \quad \mathbf{f}^{(i)} = |e_{iq}|\bar{q}^{(i)} + \sigma|e_{iT}|\bar{T}^{(i)} \quad (13)$$

Clearly, the LCM is a coarse zeroth-order DG model with the inverse of thermal resistance chosen as the element-wise penalty factors. Or conversely, the DG model is a refined version of LCM via *hp*-adaptation.

The FOM and RPM represent two extremes in the modeling fidelity and computational cost spectrum. On one hand, the FOM is the most accurate but computationally expensive to evaluate due to the fine mesh discretizations for both the temperature and displacement fields, leading to possibly millions of state variables. On the other hand, the RPM considers only the average temperature of the material as the state variable, considerably reducing the computational cost, but sacrificing local temperature information and thus neglecting higher-order effects due to mesh motion. Thus, neither the FOM nor the RPM is a universal approach for real-world analysis, design, and optimization tasks for ablating TPS, where thousands of high-fidelity model evaluations may be necessary. This issue motivates the development of the PIROM, which can achieve the fidelity of FOM at a computational cost close to the RPM, while maintaining the generalizability to model parameters.

3 Physics-Infused Reduced-Order Modeling

The formulation of PIROM for ablating TPS starts by connecting the FOM, i.e., DG-FEM, and the RPM, i.e., the LCM, via a coarse-graining procedure. This procedure pinpoints the missing dynamics in the LCM when compared to DG-FEM. Subsequently, the Mori-Zwanzig (MZ) formalism is employed to determine the model form for the missing dynamics in PIROM. Lastly, the data-driven identification of the missing dynamics in PIROM is presented.

3.1 Deriving the Reduced-Physics Model via Coarse-Graining

The LCM is derived from a full-order DG on a fine mesh via coarse graining. This process constraints the trial function space of a full-order DG model to a subset of piece-wise constants, so that the variables \mathbf{u} , matrices \mathbf{A} , \mathbf{B} , and \mathbf{C} , and forcing vector \mathbf{f} are all ap-

proximated using a single state associated to the average temperature. The details of the projection are described next.

3.1.1 Coarse-Graining of States

Consider a DG model as in eq. (7) for M elements and an LCM as in eq. (8) for N components; clearly $M \gg N$. Let $\mathcal{V}_j = \{i | E_i \in \Omega_j\}$ be the indices of the elements belonging to the j -th component, so $E_i \in \Omega_j$ for all $i \in \mathcal{V}_j$. The number of elements in the j -th component is $|\mathcal{V}_j|$. The average temperature on Ω_j is,

$$\bar{u}_j = \frac{1}{|\Omega_j|} \sum_{i \in \mathcal{V}_j} \int_{E(i)} \phi^{(i)}(x)^T \mathbf{u}^{(i)} d\Omega = \frac{1}{|\Omega_j|} \sum_{i \in \mathcal{V}_j} |E_i| \boldsymbol{\varphi}_i^{j\top} \mathbf{u}^{(i)}, \quad j = 1, 2, \dots, N \quad (14)$$

where $|\Omega_j|$ and $|E_i|$ denote the area ($d = 2$) or volume ($d = 3$) of component j and element i , respectively. The orthogonal basis functions are defined as $\boldsymbol{\varphi}_i^{j\top} = [1, 0, \dots, 0]^\top \in \mathbb{R}^P$.

Conversely, given the average temperatures of the N components, $\bar{\mathbf{u}}$, the states of an arbitrary element E_i is written as,

$$\mathbf{u}^{(i)} = \sum_{k=1}^N \boldsymbol{\varphi}_i^k \bar{u}_k + \delta \mathbf{u}^{(i)}, \quad i = 1, 2, \dots, M \quad (15)$$

where $\boldsymbol{\varphi}_i^k = 0$ if $i \notin \mathcal{V}_k$, and $\delta \mathbf{u}^{(i)}$ represents the deviation from the average temperature and satisfies the orthogonality condition $\boldsymbol{\varphi}_i^{k\top} \delta \mathbf{u}^{(i)} = 0$ for all k .

Equations eqs. (14) and (15) are combined and written in matrix form as,

$$\bar{\mathbf{u}} = \boldsymbol{\Phi}^+ \mathbf{u}, \quad \mathbf{u} = \boldsymbol{\Phi} \mathbf{u} + \delta \mathbf{u} \quad (16)$$

where $\boldsymbol{\Phi} \in \mathbb{R}^{MP \times N}$ is a matrix of $M \times N$ blocks, with the (i, j) -th block as $\boldsymbol{\varphi}_i^j$, $\boldsymbol{\Phi}^+ \in \mathbb{R}^{N \times MP}$ is the left inverse of $\boldsymbol{\Phi}$, with the (i, j) -th block as $\boldsymbol{\varphi}_i^{j+} = \frac{|E_i|}{|\Omega_j|} \boldsymbol{\varphi}_i^{j\top}$, and $\delta \mathbf{u}$ is the collection of deviations. By their definitions, $\boldsymbol{\Phi}^+ \boldsymbol{\Phi} = \mathbf{I}$ and $\boldsymbol{\Phi}^+ \delta \mathbf{u} = \mathbf{0}$.

3.1.2 Coarse-Graining of Dynamics

Next, consider a function of states in the form of $\mathbf{M}(\mathbf{u}) \mathbf{g}(\mathbf{u})$, where $\mathbf{g} : \mathbb{R}^{MP} \rightarrow \mathbb{R}^{MP}$ is a vector-valued function, and $\mathbf{M} : \mathbb{R}^{MP} \rightarrow \mathbb{R}^{p \times MP}$ is a matrix-valued function with an arbitrary dimension p . Define the projection matrix $\mathbf{P} = \boldsymbol{\Phi} \boldsymbol{\Phi}^+$ and the projection operator

177 \mathcal{P} as,

$$\begin{aligned}\mathcal{P} [\mathbf{M}(\mathbf{u})\mathbf{g}(\mathbf{u})] &= \mathbf{M}(\mathbf{P}\mathbf{u})\mathbf{g}(\mathbf{P}\mathbf{u}) \\ &= \mathbf{M}(\Phi\bar{\mathbf{u}})\mathbf{g}(\Phi\bar{\mathbf{u}})\end{aligned}\tag{17}$$

178 so that the resulting function depends only on the average temperatures $\bar{\mathbf{u}}$. Correspondingly,
179 the residual operator $\mathcal{Q} = \mathcal{I} - \mathcal{P}$, and $\mathcal{Q} [\mathbf{M}(\mathbf{u})\mathbf{g}(\mathbf{u})] = \mathbf{M}(\mathbf{u})\mathbf{g}(\mathbf{u}) - \mathbf{M}(\Phi\bar{\mathbf{u}})\mathbf{g}(\Phi\bar{\mathbf{u}})$. When
180 the function is not separable, the projection operator is simply defined as $\mathcal{P} [\mathbf{g}(\mathbf{u})] = \mathbf{g}(\mathbf{P}\mathbf{u})$.

181 Subsequently, the operators defined above are applied to coarse-grain the dynamics. First,
182 write the DG-FEM in eq. (7) as,

$$\dot{\mathbf{u}} = \mathbf{A}(\mathbf{u})^{-1}\mathbf{B}(\mathbf{u})\mathbf{u} + \mathbf{A}(\mathbf{u})^{-1}\mathbf{C}(\mathbf{u})\mathbf{u} + \mathbf{A}(\mathbf{u})^{-1}\mathbf{f}(t)\tag{18}$$

183 and multiply both sides by Φ^+ to obtain,

$$\Phi^+\dot{\mathbf{u}} = \Phi^+ (\Phi\dot{\bar{\mathbf{u}}} + \delta\dot{\mathbf{u}}) = \dot{\bar{\mathbf{u}}} = \Phi^+\mathbf{r}(\mathbf{u}, t)\tag{19}$$

184 Apply the projection operator \mathcal{P} and the residual operator \mathcal{Q} to the right-hand side to obtain,

$$\dot{\bar{\mathbf{u}}} = \mathcal{P} [\Phi^+\mathbf{r}(\mathbf{u}, t)] + \mathcal{Q} [\Phi^+\mathbf{r}(\mathbf{u}, t)] \equiv \mathbf{r}^{(1)}(\bar{\mathbf{u}}, t) + \mathbf{r}^{(2)}(\bar{\mathbf{u}}, t)\tag{20}$$

185 where $\mathbf{r}^{(1)}(\bar{\mathbf{u}}, t)$ is resolved dynamics that depends on $\bar{\mathbf{u}}$ only, and $\mathbf{r}^{(2)}(\bar{\mathbf{u}}, t)$ is the un-resolved
186 or residual dynamics. Detailed derivations and analysis of $\mathbf{r}^{(1)}(\bar{\mathbf{u}}, t)$ and $\mathbf{r}^{(2)}(\bar{\mathbf{u}}, t)$ can be
187 found in the Appendix.

188 It follows from Ref. [x](#) that the resolved dynamics is exactly the LCM, where the advection
189 term reduces to zero, i.e., $\bar{\mathbf{C}}(\bar{\mathbf{u}}) = \mathbf{0}$ as shown in the Appendix. Using the notation from
190 eq. (8), it follows that,

$$\begin{aligned}\mathbf{r}^{(1)}(\bar{\mathbf{u}}, t) &= \bar{\mathbf{A}}(\bar{\mathbf{u}})^{-1}\bar{\mathbf{B}}(\bar{\mathbf{u}})\bar{\mathbf{u}} + \bar{\mathbf{A}}(\bar{\mathbf{u}})^{-1}\bar{\mathbf{C}}(\bar{\mathbf{u}})\bar{\mathbf{u}} + \bar{\mathbf{A}}(\bar{\mathbf{u}})^{-1}\bar{\mathbf{f}}(\bar{\mathbf{u}}) \\ &= \bar{\mathbf{A}}(\bar{\mathbf{u}})^{-1}\bar{\mathbf{B}}(\bar{\mathbf{u}})\bar{\mathbf{u}} + \bar{\mathbf{A}}(\bar{\mathbf{u}})^{-1}\bar{\mathbf{f}}(t)\end{aligned}\tag{21}$$

191 where the following relations hold,

$$\bar{\mathbf{A}}(\bar{\mathbf{u}}) = \mathbf{W} (\Phi^+ \mathbf{A} (\Phi\bar{\mathbf{u}})^{-1} \Phi)^{-1} \quad \bar{\mathbf{C}}(\bar{\mathbf{u}}) = \mathbf{0}\tag{22a}$$

$$\bar{\mathbf{B}}(\bar{\mathbf{u}}) = \mathbf{W}\Phi^+\mathbf{B}(\Phi\bar{\mathbf{u}})\Phi \quad \bar{\mathbf{f}}(t) = \mathbf{W}\Phi^+\mathbf{f}\tag{22b}$$

192 where $\mathbf{W} \in \mathbb{R}^{N \times N}$ is a diagonal matrix with the i -th element as $[\mathbf{W}]_{ii} = |\mathcal{V}_k|$ if $i \in$
193 \mathcal{V}_k . As shown in the Appendix, the examination of the second residual term $\mathbf{r}^{(2)}(\bar{\mathbf{u}}, t)$ in

eq. (20) reveals the physical sources of missing dynamics in the LCM: the approximation of non-uniform temperature within each component as a constant, and the elimination of the advection term due to coarse-graining.

In sum, the above results not only show that the LCM is a result of coarse-graining of the full-order DG-FEM, but also reveal the discrepancies between the LCM and the DG-FEM. In the subsequent section, the discrepancies will be corrected to produce the proposed PIROM.

3.2 Formulation of Reduced-Order Model

The Mori-Zwanzig (MZ) formalism is an operator-projection technique used to derive ROMs for high-dimensional dynamical systems, especially in statistical mechanics and fluid dynamics [Parish,Duraisamy](#). It provides an exact reformulation of the full-order dynamics in terms of a subset of resolved variables. The proposed ROM is subsequently developed based on such reformulation. Equation eq. (20) shows that the DG-FEM dynamics can be decomposed into the resolved dynamics $\mathbf{r}^{(1)}(\mathbf{u}, t)$ and the orthogonal dynamics $\mathbf{r}^{(2)}(\mathbf{u}, t)$, in the sense of $\mathcal{P}\mathbf{r}^{(2)} = 0$. In this case, the MZ formalism can be invoked to express the dynamics $\bar{\mathbf{u}}$ in terms of $\bar{\mathbf{u}}$ alone as the projected Generalized Langevin Equation (GLE) [Parish,Duraisamy](#),

$$\dot{\bar{\mathbf{u}}}(t) = \mathbf{r}^{(1)}(\bar{\mathbf{u}}, t) + \int_0^t \tilde{\boldsymbol{\kappa}}(t, s, \bar{\mathbf{u}}) ds \quad (23)$$

where the first term is Markovian, and the integral term is referred to as the memory. The integral term is non-Markovian, accounting for impact of past resolved states on the current states through their interactions with the un-resolved states.

Next, to further inform the subsequent derivation of the ROM, the kernel $\tilde{\boldsymbol{\kappa}}$ is examined via a leading-order expansion, based on prior work [x](#); this can be viewed as an analog of zeroth-order holding in linear system theory with a sufficiently small time step. In this case, the memory kernel is approximated as,

$$\tilde{\boldsymbol{\kappa}}(t, s, \bar{\mathbf{u}}) \approx \mathbf{r}^{(1)}(\bar{\mathbf{u}}, t) \cdot \nabla_{\bar{\mathbf{u}}} \mathbf{r}^{(2)}(\Phi \bar{\mathbf{u}}, t) \quad (24)$$

Note that the terms in $\mathbf{r}^{(1)}$ have a common factor $\bar{\mathbf{A}}^{-1}$; this motivates the following heuristic

218 modification of the model form in eq. (23),

$$\dot{\mathbf{u}} = \mathbf{r}^{(1)}(\bar{\mathbf{u}}, t) + \bar{\mathbf{A}}^{-1}(\bar{\mathbf{u}}) \int_0^t \boldsymbol{\kappa}(t, s, \bar{\mathbf{u}}) ds \quad (25a)$$

$$\bar{\mathbf{A}}(\bar{\mathbf{u}}) \dot{\mathbf{u}} = \bar{\mathbf{B}}(\bar{\mathbf{u}}) \bar{\mathbf{u}} + \bar{\mathbf{f}}(t) + \int_0^t \boldsymbol{\kappa}(t, s, \bar{\mathbf{u}}) ds \quad (25b)$$

219 where the original kernel $\tilde{\boldsymbol{\kappa}}$ is effectively normalized by $\bar{\mathbf{A}}^{-1}$. Intuitively, such choice of kernel
 220 reduces its dependency on the averaged material properties, and simplifies the subsequent
 221 design of model form.

222 Subsequently, the hidden states are introduced to “Markovianize” the system eq. (23).
 223 In this manner, eq. (25b) is converted into a pure state-space model, with the functional
 224 form of the LCM retained; since LCM is a physics-based model, then it encodes the phys-
 225 ical information and retains explicit parametric dependence of the problem. Consider the
 226 representation of the kernel as a finite sum of simpler functions, e.g., exponentials,

$$\boldsymbol{\kappa}(t, s, \bar{\mathbf{u}}) = \sum_{j=1}^m \mathcal{K}_j(t, s, \bar{\mathbf{u}}) [\mathbf{p}_j + \mathbf{d}_j(\bar{\mathbf{u}})] \phi_j(s, \bar{\mathbf{u}}) \quad (26)$$

227 where,

$$\mathcal{K}_j(t, s, \bar{\mathbf{u}}) = e^{-\int_s^t (\lambda_j + e_j(\bar{\mathbf{u}})) d\tau}, \quad \phi_j(s, \bar{\mathbf{u}}) = \mathbf{q}_j^\top \bar{\mathbf{u}}(s) + \mathbf{g}_j(\bar{\mathbf{u}})^\top \bar{\mathbf{u}}(s) + \mathbf{r}_j^\top \bar{\mathbf{f}}(s) \quad (27)$$

228 with suitable coefficients $\mathbf{p}_j, \mathbf{d}_j, \mathbf{q}_j, \mathbf{g}_j, \mathbf{r}_j \in \mathbb{R}^N$ and decay rates $\lambda_j, e_j(\bar{\mathbf{u}}) > 0$, that need to
 229 be identified from data.

230 Define the hidden states as,

$$\beta_j(t) = \int_0^t \mathcal{K}_j(s, \bar{\mathbf{u}}) \phi_j(s, \bar{\mathbf{u}}) ds \quad (28)$$

231 then through its differentiation with respect to time,

$$\dot{\beta}_j(t) = -[\lambda_j + e_j(\bar{\mathbf{u}})] \beta_j(t) + \mathbf{q}_j^\top \bar{\mathbf{u}}(t) + \mathbf{g}_j(\bar{\mathbf{u}})^\top \bar{\mathbf{u}}(t) + \mathbf{r}_j^\top \bar{\mathbf{f}}(t) \quad (29)$$

232 and the memory term becomes,

$$\int_0^t \boldsymbol{\kappa}(t, s, \bar{\mathbf{u}}) ds = \sum_{j=1}^m [\mathbf{p}_j + \mathbf{d}_j(\bar{\mathbf{u}})] \beta_j(t) \quad (30)$$

233 Then, eq. (25b) is recast as the extended Markovian system,

$$\bar{\mathbf{A}}(\bar{\mathbf{u}})\dot{\bar{\mathbf{u}}} = \bar{\mathbf{B}}(\bar{\mathbf{u}})\bar{\mathbf{u}} + [\mathbf{P} + \mathbf{D}(\bar{\mathbf{u}})]\boldsymbol{\beta} + \bar{\mathbf{f}}(t) \quad (31a)$$

$$\dot{\boldsymbol{\beta}} = [-\boldsymbol{\Lambda} + \mathbf{E}(\bar{\mathbf{u}})]\boldsymbol{\beta} + [\mathbf{Q} + \mathbf{G}(\bar{\mathbf{u}})]\bar{\mathbf{u}} + \mathbf{R}\bar{\mathbf{f}}(t) \quad (31b)$$

234 where,

$$\boldsymbol{\Lambda} = \text{diag}(\lambda_1, \lambda_2, \dots, \lambda_m) \in \mathbb{R}^{N \times m}, \quad \mathbf{P} = [\mathbf{p}_1, \mathbf{p}_2, \dots, \mathbf{p}_m] \in \mathbb{R}^{N \times m} \quad (32a)$$

$$\mathbf{D}(\bar{\mathbf{u}}) = [\mathbf{d}_1(\bar{\mathbf{u}}), \mathbf{d}_2(\bar{\mathbf{u}}), \dots, \mathbf{d}_m(\bar{\mathbf{u}})] \in \mathbb{R}^{N \times m}, \quad \mathbf{Q} = [\mathbf{q}_1, \mathbf{q}_2, \dots, \mathbf{q}_m] \in \mathbb{R}^{N \times m} \quad (32b)$$

$$\mathbf{G}(\bar{\mathbf{u}}) = [\mathbf{g}_1(\bar{\mathbf{u}}), \mathbf{g}_2(\bar{\mathbf{u}}), \dots, \mathbf{g}_m(\bar{\mathbf{u}})] \in \mathbb{R}^{N \times m}, \quad \mathbf{R} = [\mathbf{r}_1, \mathbf{r}_2, \dots, \mathbf{r}_m] \in \mathbb{R}^{N \times m} \quad (32c)$$

$$\mathbf{E}(\bar{\mathbf{u}}) = \text{diag}(e_1(\bar{\mathbf{u}}), e_2(\bar{\mathbf{u}}), \dots, e_m(\bar{\mathbf{u}})) \in \mathbb{R}^{m \times m} \quad (32d)$$

235 Since the hidden states $\boldsymbol{\beta}$ serve as the memory, their initial conditions are set to zero, i.e.,
 236 $\boldsymbol{\beta}(t_0) = \mathbf{0}$, no memory at the beginning. The physics-infused model in eq. (31b) retains the
 237 structure of the LCM, while the hidden states account for missing physics through corrections
 238 to the stiffness and advection matrices, as well as the forcing term.

239 Lastly, denote the collection of resolved and hidden states as $\mathbf{y} = [\bar{\mathbf{u}}, \boldsymbol{\beta}]^T \in \mathbb{R}^{n_y}$ with
 240 $n_y = N + m$, then the proposed PIROM is summarized as,

$$\tilde{\mathbf{A}}\dot{\mathbf{y}} = [\tilde{\mathbf{B}} + \tilde{\mathbf{C}}]\mathbf{y} + \mathbf{H}\bar{\mathbf{f}}(t) \quad (33a)$$

$$\mathbf{z} = \mathbf{M}\mathbf{y} \quad (33b)$$

241 where,

$$\tilde{\mathbf{A}} = \begin{bmatrix} \bar{\mathbf{A}}(\bar{\mathbf{u}}) & \mathbf{O} \\ \mathbf{O} & \mathbf{I} \end{bmatrix} \in \mathbb{R}^{n_y \times n_y}, \quad \tilde{\mathbf{B}} = \begin{bmatrix} \bar{\mathbf{B}}(\bar{\mathbf{u}}) & \mathbf{P} \\ \mathbf{Q} & -\boldsymbol{\Lambda} \end{bmatrix} \in \mathbb{R}^{n_y \times n_y}, \quad \tilde{\mathbf{C}} = \begin{bmatrix} \mathbf{0} & \mathbf{D}(\bar{\mathbf{u}}) \\ \mathbf{G}(\bar{\mathbf{u}}) & \mathbf{E}(\bar{\mathbf{u}}) \end{bmatrix} \in \mathbb{R}^{n_y \times n_y}, \quad (34a)$$

$$\mathbf{H} = \begin{bmatrix} \mathbf{I} \\ \mathbf{R} \end{bmatrix} \in \mathbb{R}^{n_y \times N}, \quad \mathbf{M} \in \mathbb{R}^{n_z \times n_y} \quad (34b)$$

242 In eq. (33b), the terms $\bar{\mathbf{A}}$, $\bar{\mathbf{B}}$, and $\bar{\mathbf{f}}$ are the LCM terms. The collection of matrices,

$$\boldsymbol{\Theta} = \{\mathbf{P}, \mathbf{D}(\bar{\mathbf{u}}), \mathbf{G}(\bar{\mathbf{u}}), \boldsymbol{\Lambda}, \mathbf{E}(\bar{\mathbf{u}}), \mathbf{Q}, \mathbf{G}(\bar{\mathbf{u}}), \mathbf{R}, \mathbf{M}\} \in \mathbb{R}^{n_\theta} \quad (35)$$

243 are learnable parameters to capture the memory effects. Particularly, the matrices $\mathbf{P}, \boldsymbol{\Lambda}, \mathbf{Q}, \mathbf{R}$
 244 are constant, and capture the effects of coarse graining on the stiffness and forcing matrices.
 245 The matrices $\mathbf{D}(\bar{\mathbf{u}}), \mathbf{E}(\bar{\mathbf{u}}), \mathbf{G}(\bar{\mathbf{u}})$ are state-dependent matrices, and capture the effects of

246 coarse-graining on the advection matrix. Leveraging the DG-FEM formula for the advection
 247 matrix in eq. (41c) from the Appendix, the state-dependent matrices for the i -th component
 248 are written as,

$$\mathbf{D}^{(i)}(\bar{\mathbf{u}}) = f^{(i)}(\bar{u}^{(i)})\mathbf{D}^{(i)}, \quad \mathbf{E}^{(i)}(\bar{\mathbf{u}}) = f^{(i)}(\bar{u}^{(i)})\mathbf{E}^{(i)}, \quad \mathbf{G}^{(i)}(\bar{\mathbf{u}}) = f^{(i)}(\bar{u}^{(i)})\mathbf{G}^{(i)} \quad (36)$$

249 where $f^{(i)}(\bar{u}^{(i)})$ is the surface recession velocity function in eq. (12) for the i -th component,
 250 and $\mathbf{D}^{(i)}, \mathbf{E}^{(i)}, \mathbf{G}^{(i)}$ are constant matrices to be identified from data. In eq. (33b), \mathbf{M} is a
 251 fully-populated matrix that extracts the observables, i.e., the surface temperatures, from the
 252 PIROM states \mathbf{y} . The PIROM now incorporates explicit information on the temperature-
 253 dependent material properties through the LCM matrices, as well as the surface recession
 254 velocity function through eq. (36).

A Technical Details

This appendix presents the technical details of the PIROM framework applied to the TPS ablation problem. The first section provides the mathematical details for the definition of the DG-FEM. The second section follows the projection procedures from Ref. [x](#), and demonstrates the effects of coarse-graining on the advection matrix. The third section presents the derivation of the LCM model from an energy-conservation perspective.

A.1 Full-Order Model

To obtain the full-order numerical solution, the governing equation is spatially discretized using variational principles of Discontinuous Galerkin (DG) to result in a high-dimensional system of ordinary differential equations (ODEs). The DG-FEM model is written in an element-wise form, which is beneficial for subsequent derivations of the lower-order models. Note that the choice of DG approach here is mainly for theoretical convenience in the subsequent coarse-graining formulation. In the numerical results, the full-order TPS ablation simulations is computed using standard FEM instead, and the equivalence between DG and standard FEM is noted upon their convergence.

A.1.1 Domain Discretization

Consider a conforming mesh partition of the domain, as shown in Fig. [DOMAIN](#), where each element belongs to one and only one component. Denote the collection of all M elements as $\{E_i\}_{i=1}^M$. To ease the description of the DG model, a graph structure is employed. The elements are treated as vertices, the set of which is denoted $\mathcal{V} = \{m\}_{m=1}^M$. Two neighboring elements, E_i and E_j , are connected by an edge (i, j) , and the shared boundary between them is denoted e_{ij} . The collection of all edges are denoted \mathcal{E} , and \mathcal{G} is referred to as a graph. In the graph, the edges are undirected, meaning if $(i, j) \in \mathcal{E}$ then $(j, i) \in \mathcal{E}$. Furthermore, denote the neighbors of the i -th element as $\mathcal{N}_i = \{j | (i, j) \in \mathcal{E}\}$. Lastly, for the ease of notation, introduce two special indices: T for the boundary of an element that overlaps with the Dirichlet boundary condition, and similarly q for the Neumann boundary condition.

A.1.2 Weak Form of Discontinuous Galerkin Method

Choosing appropriate basis functions ϕ_k and ϕ_l and using the Interior Penalty Galerkin (IPG) scheme [?], the variational bilinear form for eq. (1a) is,

$$\sum_{i=1}^M a_{\epsilon,i}(\phi_k, \phi_l) = \sum_{i=1}^M L_i(\phi_k) \quad (37)$$

where ϵ is an user-specified parameter and,

$$a_{\epsilon,i}(\phi_k, \phi_l) = \int_{E^{(i)}} \left(\rho c_p \phi_k \frac{\partial \phi_l}{\partial t} + \nabla \phi_k \cdot (\mathbf{k} \nabla \phi_l) - \rho c_p \phi_k \mathbf{v} \cdot \nabla \phi_l \right) dE^{(i)} \quad (38a)$$

$$\begin{aligned} &= - \sum_{j \in \mathcal{N}_i \cup \{T_b\}} \int_{e_{ij}} \{\mathbf{k} \nabla \phi_k \cdot \mathbf{n}\} [\phi_l] de_{ij} + \epsilon \sum_{j \in \mathcal{N}_i \cup \{T_b\}} \int_{e_{ij}} \{\mathbf{k} \nabla \phi_l \cdot \mathbf{n}\} [\phi_k] de_{ij} \\ &+ \sigma \sum_{j \in \mathcal{N}_i \cup \{T_b\}} \int_{e_{ij}} [\phi_k] [\phi_l] de_{ij} \end{aligned} \quad (38b)$$

$$L_i(v) = \epsilon \sum_{j \in \mathcal{N}_i \cup \{T_b\}} \int_{e_{ij}} (\mathbf{k} \nabla \phi_l \cdot \mathbf{n}) T_b de_{ij} + \int_{e_{iq}} \phi_k q_b de_{iq} + \sigma \int_{e_{iT}} \phi_k T_b de_{iT} \quad (38c)$$

In the bi-linear form above, the notations $[]$ and $\{\}$ are respectively the jumps and averages at the boundary e_{ij} share by two elements E_i and E_j ,

$$[u] = u|_{E_i} - u|_{E_j}, \quad \{u\} = \frac{1}{2} (u|_{E_i} + u|_{E_j}), \quad \text{for } x \in e_{ij} = E_i \cap E_j$$

Furthermore, in the bi-linear form, the terms associated with σ are introduced to enforce the Dirichlet boundary conditions; σ is a penalty factor whose value can depend on the size of an element. Depending on the choice of ϵ , the bi-linear form corresponds to symmetric IPG ($\epsilon = -1$), non-symmetric IPG ($\epsilon = 1$), and incomplete IPG ($\epsilon = 0$). All these schemes are consistent with the original PDE and have similar convergence rate with respect to mesh size. In the following derivations, the case $\epsilon = 0$ is chosen for the sake of simplicity.

A.1.3 Discontinuous Galerkin Model

Next, the DG-based model is written in an element-wise form. For the i -th element, use a set of P trial functions to represent the temperature as in eq. (5). Without loss of generality, the trial functions are assumed to be orthogonal, so that $\int_{E^{(i)}} \phi_k^{(i)}(x) \phi_l^{(i)}(x) dx = |E^{(i)}| \delta_{kl}$, where $|E^{(i)}|$ is the area ($n_d = 2$) or volume ($n_d = 3$) of the i -th element, and δ_{kl} is the Kronecker delta.

Using test functions same as trial functions, the dynamics $\mathbf{u}^{(i)}$ is obtained by evaluating

the element-wise bi-linear forms,

$$a_{\epsilon,i}(\phi_k^{(i)}, T^{(i)}) = L_i(\phi_k^{(i)}), \quad k = 1, 2, \dots, P \quad (39)$$

The above procedure yields,

$$\mathbf{A}^{(i)} \dot{\mathbf{u}}^{(i)} = (\mathbf{B}^{(i)} + \mathbf{C}^{(i)}(t)) \mathbf{u}^{(i)} + \sum_{j \in \mathcal{N}_i \cup \{T_b\}} (\mathbf{B}_{ij}^{(i)} \mathbf{u}^{(i)} + \mathbf{B}_{ij}^{(j)} \mathbf{u}^{(j)}) + \mathbf{f}^{(i)}(t) \quad (40)$$

where for $k, l = 1, 2, \dots, P$,

$$[\mathbf{A}^{(i)}]_{kl} = \int_{E^{(i)}} \rho c_p \phi_k^{(i)} \phi_l^{(i)} dE^{(i)} \quad (41a)$$

$$[\mathbf{B}^{(i)}]_{kl} = - \int_{E^{(i)}} (\nabla \phi_k^{(i)}) \cdot (\mathbf{k} \nabla \phi_l^{(i)}) dE^{(i)} \quad (41b)$$

$$[\mathbf{C}^{(i)}]_{kl} = \int_{E^{(i)}} \rho c_p \phi_k^{(i)} \mathbf{v}^{(i)} \cdot \nabla \phi_l^{(i)} dE^{(i)} \quad (41c)$$

$$[\mathbf{B}_{ij}^{(i)}] = \int_{e_{ij}} \left\{ \mathbf{k} \nabla \phi_k^{(i)} \cdot \hat{n} \right\} \phi_l^{(i)} - \sigma [\phi_k^{(i)}] \phi_l^{(i)} de_{ij} \quad (41d)$$

$$[\mathbf{B}_{ij}^{(j)}] = \int_{e_{ij}} - \left\{ \mathbf{k} \nabla \phi_k^{(i)} \cdot \hat{n} \right\} \phi_l^{(j)} + \sigma [\phi_k^{(i)}] \phi_l^{(j)} de_{ij} \quad (41e)$$

$$[\mathbf{f}^{(i)}]_k = \int_{e_{iq}} \phi_k^{(i)} q_b de_{iq} + \sigma \int_{e_{iT}} \phi_k^{(i)} de_{iT} \quad (41f)$$

The matrices $\mathbf{A}^{(i)} \in \mathbb{R}^{P \times P}$, $\mathbf{B}^{(i)} \in \mathbb{R}^{P \times P}$, and $\mathbf{C}^{(i)} \in \mathbb{R}^{P \times P}$ are respectively the capacitance, conductivity, and advection matrices for element i . These matrices depend on ρ , c_p , \mathbf{k} , and \mathbf{v} , and hence can be non-linear functions of $\mathbf{u}^{(i)}$. Since the trial functions are orthogonal, if ρc_p is constant within an element, $\mathbf{A}^{(i)}$ is diagonal; otherwise, \mathbf{A}_i is symmetric and positive definite as $\rho c_p > 0$.

For compactness, the element-wise model in eq. (40) is also written in matrix form,

$$\mathbf{A}(\dot{\mathbf{u}}) = [\mathbf{B}(\mathbf{u}) + \mathbf{C}(t, \mathbf{u})] \mathbf{u} + \mathbf{f}(t) \quad (42)$$

where $\mathbf{u} = [\mathbf{u}^{(1)}, \mathbf{u}^{(2)}, \dots, \mathbf{u}^{(M)}]^T \in \mathbb{R}^{MP}$ includes all DG variables, $\mathbf{f} = [\mathbf{f}^{(1)}, \mathbf{f}^{(2)}, \dots, \mathbf{f}^{(M)}]^T \in \mathbb{R}^{MP}$, \mathbf{A} and \mathbf{C} are matrices of M diagonal blocks whose i -th blocks are $\mathbf{A}^{(i)}$ and $\mathbf{C}^{(i)}$, and \mathbf{B} is a matrix of $M \times M$ blocks whose (i, j) -th block is,

$$\mathbf{B}_{ij} = \begin{cases} \mathbf{B}^{(i)} + \sum_{j \in \mathcal{N}_i \cup \{T_b\}} \mathbf{B}_{ij}^{(i)}, & i = j \\ \mathbf{B}_{ij}^{(j)}, & i \neq j \end{cases} \quad (43)$$

312 The dependency of \mathbf{A} , \mathbf{B} , and \mathbf{C} on \mathbf{u} is explicitly noted in eq. (42), which is the source of
 313 non-linearity in the current TPS problem. Moreover, the mesh velocity \mathbf{v} varies with space
 314 and time, and thus the advection matrix \mathbf{C} varies with time as a function of q_b .

315 A.2 Coarse-Graining of Dynamics

316 The LCM is obtained by coarse-graining the full-order DG-FEM. This coarse-graining proce-
 317 dure produces resolved $\mathbf{r}^{(1)}(\mathbf{u}, t)$ and residual $\mathbf{r}^{(2)}(\mathbf{u}, t)$ dynamics as in eq. (20). This section
 318 presents the detail derivations and magnitude analysis for the resolved and residual dynam-
 319 ics.

320 A.2.1 Resolved Dynamics

321 Using eq. (17), the resolved dynamics is computed as follows,

$$\mathbf{r}^{(1)}(\mathbf{u}, t) = \mathcal{P} [\Phi^+ \mathbf{A}(\mathbf{u})^{-1} (\mathbf{B}(\mathbf{u})\mathbf{u} + \mathbf{C}(t, \mathbf{u})\mathbf{u} + \mathbf{f}(t, \mathbf{u}))] \quad (44a)$$

$$\begin{aligned} &= \Phi^+ \mathbf{A}(\mathbf{P}\mathbf{u})^{-1} \mathbf{P}\mathbf{B}(\mathbf{P}\mathbf{u}) \mathbf{P}\mathbf{u} + \Phi^+ \mathbf{A}(\mathbf{P}\mathbf{u})^{-1} \mathbf{P}\mathbf{C}(t, \mathbf{P}\mathbf{u}) \mathbf{P}\mathbf{u} \\ &\quad + \Phi^+ \mathbf{A}(\mathbf{P}\mathbf{u})^{-1} \mathbf{P}\mathbf{f}(t, \mathbf{P}\mathbf{u}) \end{aligned} \quad (44b)$$

$$\begin{aligned} &= \underbrace{\Phi^+ \mathbf{A}(\Phi\bar{\mathbf{u}})^{-1} \Phi}_{\#1} \underbrace{\Phi^+ \mathbf{B}(\Phi\bar{\mathbf{u}}) \Phi}_{\#2} \bar{\mathbf{u}} + \Phi^+ \mathbf{A}(\Phi\bar{\mathbf{u}})^{-1} \Phi \underbrace{\Phi^+ \mathbf{C}(t, \Phi\bar{\mathbf{u}}) \Phi}_{\#3} \bar{\mathbf{u}} \\ &\quad + \Phi^+ \mathbf{A}(\Phi\bar{\mathbf{u}})^{-1} \Phi \underbrace{\Phi^+ \mathbf{f}(t, \Phi\bar{\mathbf{u}})}_{\#4} \end{aligned} \quad (44c)$$

322 Detailed derivations for the #1, #2, and #4 terms can be found in Ref. [x](#). The effects of
 323 coarse-graining on the advection term #3 are analyzed next.

324 **Term #3** The $\mathbf{C}(t, \mathbf{u}) \in \mathbb{R}^{MP \times MP}$ matrix contains M diagonal of size $P \times P$, since the
 325 basis functions are defined locally on each element. Therefore, $[\mathbf{C}(t, \mathbf{u})]_{ij} = \mathbf{0}$ for all $i \neq j$
 326 with $i, j = 1, 2, \dots, M$. It follows that for $k, l = 1, 2, \dots, N$,

$$[\Phi^+ \mathbf{C}(t, \Phi\bar{\mathbf{u}}) \Phi]_{kl} = \sum_{i=1}^M \sum_{j=1}^M \varphi_i^{k+} [\mathbf{C}(t, \Phi\bar{\mathbf{u}})]_{ij} \varphi_j^l \quad (45a)$$

$$= \sum_{i=1}^M \varphi_i^{k+} [\mathbf{C}(t, \Phi\bar{\mathbf{u}})]_{ii} \varphi_i^l \quad (45b)$$

$$= \sum_{i \in \mathcal{V}_k} \varphi_i^{k+} [\mathbf{C}(t, \Phi\bar{\mathbf{u}})]_{ii} \varphi_i^l \quad (45c)$$

where in the second row, the fact that $[\mathbf{C}(t, \mathbf{u})]_{ij} = 0$ for all $i \neq j$ is used, and in the last row, the fact that $\varphi_i^{k+} = 0$ for all $i \notin \mathcal{V}_k$ is used. Now, considering that $[\mathbf{C}(t, \mathbf{u})]_{ii}$ has a (1, 1)-th zero element, i.e., $[C_{11}(t, \Phi \bar{\mathbf{u}})]_{ii} = 0$, and that if $k \neq l$ then $i \notin \mathcal{V}_l$ and thus $\varphi_i^l = 0$, it follows that for some index $i \in \mathcal{V}_k$,

$$\varphi_i^{k+} [\mathbf{C}(t, \Phi \bar{\mathbf{u}})]_{ii} \varphi_i^l = \varphi_i^{k+} [\mathbf{C}(t, \Phi \bar{\mathbf{u}})]_{ii} \varphi_i^k = \frac{|E_i|}{|\Omega_k|} [C_{11}(t, \Phi \bar{\mathbf{u}})]_{ii} = 0 \quad (46)$$

The matrix $[\Phi^+ \mathbf{C}(t, \Phi \bar{\mathbf{u}}) \Phi]_{kl} = 0$ for all $k, l = 1, 2, \dots, N$, and thus,

$$\bar{\mathbf{C}}(t, \bar{\mathbf{u}}) = \Phi^+ \mathbf{C}(t, \Phi \bar{\mathbf{u}}) \Phi = \mathbf{0} \quad (47)$$

as indicated by the LCM in eq. (8).

A.2.2 Magnitude Analysis for Residual Dynamics

Next, the magnitude of the residual dynamics $\mathbf{r}^{(2)}(\mathbf{u}, t)$ is analyzed to pinpoint the missing physics in the LCM. By definition,

$$\mathbf{r}^{(2)}(\mathbf{u}, t) = \dot{\bar{\mathbf{u}}} - \mathbf{r}^{(1)}(\bar{\mathbf{u}}, t) \quad (48a)$$

$$= \Phi^+ \mathbf{r}(\mathbf{u}, t) - \mathbf{r}^{(1)}(\mathbf{u}, t) \quad (48b)$$

$$\begin{aligned} &= \underbrace{\Phi^+ \mathbf{A}(\mathbf{u})^{-1} \mathbf{B}(\mathbf{u}) \mathbf{u} - \bar{\mathbf{A}}(\bar{\mathbf{u}})^{-1} \bar{\mathbf{B}}(\bar{\mathbf{u}}) \bar{\mathbf{u}}}_{\#1} + \underbrace{\Phi^+ \mathbf{A}(\mathbf{u})^{-1} \mathbf{C}(t, \mathbf{u}) \mathbf{u} - \bar{\mathbf{A}}(\bar{\mathbf{u}})^{-1} \bar{\mathbf{C}}(t, \bar{\mathbf{u}}) \bar{\mathbf{u}}}_{\#2} \\ &\quad + \underbrace{\Phi^+ \mathbf{A}(\mathbf{u})^{-1} \mathbf{f}(t) - \bar{\mathbf{A}}(\bar{\mathbf{u}})^{-1} \bar{\mathbf{f}}(t)}_{\#3} \end{aligned} \quad (48c)$$

The magnitude analysis for terms #1 and #3 can be found in Ref. [x](#). The analysis for term #2 is presented next. Let $\mathbf{D}(\bar{\mathbf{u}}) = \mathbf{A}(\Phi \bar{\mathbf{u}})^{-1} \mathbf{P} \mathbf{C}(t, \Phi \bar{\mathbf{u}})$, then,

$$\Phi^+ \mathbf{A}(\mathbf{u})^{-1} \mathbf{C}(t, \mathbf{u}) \mathbf{u} - \bar{\mathbf{A}}(\bar{\mathbf{u}})^{-1} \bar{\mathbf{C}}(t, \bar{\mathbf{u}}) \bar{\mathbf{u}} \quad (49a)$$

$$= \Phi^+ \mathbf{A}(\mathbf{u})^{-1} \mathbf{C}(t, \mathbf{u}) \mathbf{u} - \Phi^+ \mathbf{A}(\Phi \bar{\mathbf{u}})^{-1} \mathbf{P} \mathbf{C}(t, \Phi \bar{\mathbf{u}}) \Phi \Phi^+ \mathbf{u} \quad (49b)$$

$$= \Phi^+ \mathbf{A}^{-1}(\mathbf{u}) \mathbf{C}(t, \mathbf{u}) \mathbf{u} - \Phi^+ \mathbf{D}(\bar{\mathbf{u}}) \Phi \Phi^+ \mathbf{u} \quad (49c)$$

$$(49d)$$

338 where $\mathbf{P} = \Phi\Phi^+$. Thus,

$$\|\Phi^+ \mathbf{A}(\mathbf{u})^{-1} \mathbf{C}(t, \mathbf{u}) \mathbf{u} - \bar{\mathbf{A}}^{-1}(\bar{\mathbf{u}}) \bar{\mathbf{C}}(t, \bar{\mathbf{u}}) \bar{\mathbf{u}}\| \quad (50a)$$

$$\leq \|\Phi^+ \mathbf{A}^{-1}(\mathbf{u}) \mathbf{C}(t, \mathbf{u}) \mathbf{u} - \Phi^+ \mathbf{D}(\bar{\mathbf{u}}) \mathbf{u}\| + \|\Phi^+ \mathbf{D}(\bar{\mathbf{u}}) \mathbf{u} - \Phi^+ \mathbf{D}(\bar{\mathbf{u}}) \Phi \Phi^+ \mathbf{u}\| \quad (50b)$$

$$\leq \|\Phi^+\| \underbrace{\|\mathbf{A}^{-1}(\mathbf{u}) \mathbf{C}(t, \mathbf{u}) \mathbf{u} - \mathbf{D}(\bar{\mathbf{u}}) \mathbf{u}\|}_{\#1} + \|\Phi^+ \mathbf{D}(\bar{\mathbf{u}})\| \underbrace{\|\mathbf{u} - \Phi \Phi^+ \mathbf{u}\|}_{\#2} \quad (50c)$$

339 where term #2 is due to the approximation of non-uniform temperature as constants, and
 340 term #1 is the error in the advection dynamics due to coarse-graining.

341 A.3 Lumped Capacitance Model

342 The following assumptions are employed: (1) the temperature in component (i) is described
 343 by a scalar time-varying average temperature $\bar{u}^{(i)}$, (2) between neighboring components (i)
 344 and (j) the heat flux is approximated as,

$$q_{ij} = \frac{\bar{u}^{(j)} - \bar{u}^{(i)}}{R_{ij}} \quad (51)$$

345 where R_{ij} is the thermal resistance. Empirically, for a component of isotropic heat conduc-
 346 tivity k , length ℓ , and cross-section area A , the thermal resistance is $R = \ell/kA$. Between
 347 components i and j , define $R_{ij} = R_i + R_j$. In addition, the heat flux due to Dirichlet
 348 boundary condition is computed as $q_{iT} = (T_b - \bar{u}^{(i)})/R_i$.

349 At component i , the dynamics of LCM are given by,

$$\int_{E^{(i)}} \rho c_p \dot{\bar{u}}^{(i)} dE^{(i)} = \left(\sum_{j \in \mathcal{N}_i} \int_{e_{ij}} \frac{\bar{u}^{(j)} - \bar{u}^{(i)}}{R_{ij}} de_{ij} \right) + \int_{e_{iq}} q_b de_{iq} + \int_{e_{iT}} \frac{T_b - \bar{u}^{(i)}}{R_i} de_{iT} \quad (52a)$$

$$\bar{A}^{(i)} \dot{\bar{u}}^{(i)} = \left(\sum_{j \in \mathcal{N}_i} \frac{|e_{ij}|}{R_{ij}} (\bar{u}^{(j)} - \bar{u}^{(i)}) \right) + |e_{iq}| \bar{q}^{(i)} + \frac{|e_{iT}|}{R_i} (\bar{T}^{(i)} - \bar{u}^{(i)}) \quad (52b)$$

$$= \sum_{j \in \mathcal{N}_i} \left(-\frac{|e_{ij}|}{R_{ij}} \bar{u}^{(i)} + \frac{|e_{ij}|}{R_{ij}} \bar{u}^{(j)} \right) + \left(-\frac{|e_{iT}|}{R_i} \bar{u}^{(i)} \right) + \left(|e_{iq}| \bar{q}^{(i)} + \frac{|e_{iT}|}{R_i} \bar{T}^{(i)} \right) \quad (52c)$$

$$= \sum_{j \in \mathcal{N}_i \cup \{T_b\}} \left(\bar{B}_{ij}^{(i)} \bar{u}^{(i)} + \bar{B}_{ij}^{(j)} \bar{u}^{(j)} \right) + \bar{f}^{(i)} \quad (52d)$$

350 where in eq. (52b) $|e|$ denotes the length ($d = 2$) or area ($d = 3$) of a component boundary
 351 e . The $\bar{A}^{(i)}$, $\bar{B}_{ij}^{(i)}$, and $\bar{B}_{ij}^{(j)}$ quantities are provided in eq. (11).

352 The lumped-mass representation for the four-component TPS is shown in Fig. 2. Let v_i

353 represent the area of the i -th element, $\overline{\rho c_{p,i}}$, the heat capacity evaluated using the average
 354 temperature $\bar{u}^{(i)}$, and $1/R_{ij} = 1/R_i(\bar{u}^{(i)}) + 1/R_j(\bar{u}^{(j)})$ the equivalent thermal resistance
 355 between elements i and j . Leveraging the formulas from eqs. (10b) and (11), the LCM
 356 matrices are given by,

$$\bar{\mathbf{A}} = \begin{bmatrix} \overline{\rho c_{p,1}} v_1 & 0 & 0 & 0 \\ 0 & \overline{\rho c_{p,2}} v_2 & 0 & 0 \\ 0 & 0 & \overline{\rho c_{p,3}} v_3 & 0 \\ 0 & 0 & 0 & \overline{\rho c_{p,4}} v_4 \end{bmatrix}, \quad (53a)$$

$$\bar{\mathbf{B}} = \begin{bmatrix} \frac{1}{R_{12}} + \frac{1}{R_{14}} & -\frac{1}{R_{12}} & 0 & -\frac{1}{R_{14}} \\ -\frac{1}{R_{12}} & \frac{1}{R_{12}} + \frac{1}{R_{24}} + \frac{1}{R_{23}} & -\frac{1}{R_{23}} & -\frac{1}{R_{24}} \\ 0 & -\frac{1}{R_{32}} & \frac{1}{R_{32}} + \frac{1}{R_{34}} & -\frac{1}{R_{34}} \\ -\frac{1}{R_{14}} & -\frac{1}{R_{24}} & -\frac{1}{R_{34}} & \frac{1}{R_{14}} + \frac{1}{R_{24}} + \frac{1}{R_{34}} \end{bmatrix}, \quad \bar{\mathbf{f}} = \begin{bmatrix} \bar{q}^{(1)} \\ \bar{q}^{(2)} \\ \bar{q}^{(3)} \\ 0 \end{bmatrix} \quad (53b)$$